Flexural testing of cellulose fiber braided composites using three dimensional digital image correlation

Can Unlusoy[1], Garrett W. Melenka[1*]

[1] Department of Mechanical Engineering, York University, Toronto, Canada

[*] Corresponding Author: gmelenka@yorku.ca

Abstract

Braided composites consist of woven fibers embedded within a matrix material. Braided structures are commonly produced using conventional materials such as carbon, glass and aramid fibers. However, natural fibers and bio-based resins may also be utilized with this manufacturing process. In this work, the flexural properties of tubular braid structures produced using bio-based materials was investigated. Braid samples were assessed using a contact free three dimensional digital image correlation (3D DIC) technique to assess the strain fields that occur in the samples due to applied flexural loads. Additionally, the bio-based structures were evaluated using micro-computed tomography (μCT) to assess the cross-sectional geometry and void content of the produced samples.

Keywords: Braided composites, natural fibers, digital image correlation, flexure, micro-computed tomography

Introduction

Braided composites are becoming alternatives to conventional composite materials in many industries due to their high strength and tailorable mechanical properties. Two-dimensional braid preforms are produced using a Maypole braiding machine which interlaces yarns around a mandrel [1]. With the continuous nature of fibers, and the interlacing achieved with the braiding pattern, braided composites allow for even load distribution and high stiffness [2]. Thanks to these favorable characteristics, braids are utilized either as reinforcements or used solely in structural components. Tubular cross sections are especially common to see due to their relatively simple manufacturing process. Among many adjustable manufacturing parameters that make braided composites highly customizable, braid angle, θ, is a major factor and its effect on mechanical properties has been of interest in previous studies [3], [4]. Braid angle is defined as the angle of the braid yarns relative to the longitudinal axis of the braid mandrel. In these studies, the tensile, flexural, and torsional behavior of conventional braided composite structures has been investigated.

Extensive testing of braided composites mechanical properties under different types of loading and environments is necessary before their widespread industrial adoption. Behavior of tubular braided composites manufactured using conventional materials under tension, torsion, and bending have been experimentally observed by several authors [3]–[5]. Tensile testing of natural fiber braided composites was performed by Qamhia *et al.* [6] using flat braided specimens and tensile

tests on tubular braided composites manufactured with natural fibers and bio-resins have been conducted by Bruni-Bossio *et al.* [7], [8]. Braided composites are also preferable from an environmental point of view as the use of bio-based materials make their production sustainable. Natural fibers in composite structures have been reviewed by Saheb et al. [9]. Bio-based materials have not been thoroughly explored for braided structures therefore, mechanical testing and evaluation of these materials is necessary to support commercial adoption.

Bending is yet another type of loading that structural components are commonly subjected to. Previously, energy absorption behavior of C-shaped braided composite frames under 4-point bending was investigated by Sturm *et al.* [10] and an increase in mass specific energy absorption was observed with increasing braid angle where braiding angles ranging from 45 to 60° were examined. Damage progression on the 3-point loading of braided composite landing gears has also been studied and experimental observations were verified with an FEA model [11]. Potluri *et al*. has examined the bending behavior of biaxial and triaxial tubular braided composites of various braid angles and developed a model based on a modified laminate theory to predict flexural moduli and rigidity values [4].

Presently, the strain fields of braided composite structures under flexural loading have not been investigated. Two-dimensional digital image correlation (2D DIC) technique has been utilized in many studies to obtain full-field strains of specimens using flexural loading. For example, Liu *et al.* used 2D DIC to obtain strain maps of nuclear graphite specimens subjected to 4-point bending loads, whereas Planques *et al.* observed 3-point bending of thermal barrier coatings using 2D DIC [12], [13]. Flexural modulus is a material property associated with bending that must be determined experimentally as it differs from elastic modulus under non-ideal conditions. Voiconi *et al.* has used 2D DIC to calculate flexural moduli of rigid PUR foams and reported that moduli calculated with DIC are approximately the same as the values obtained using the equations given in the industry testing standard ASTM D790 [14]. The standard describes the 3-point bending test methods for plastic or composite specimens with rectangular cross sections. The equations provided in the standard for moduli of elasticity are not directly applicable to tubular braided composites due to the non-uniform geometry and cross sectional shape. The cross-sectional geometry of braided composite structures can be assess using a non-destructive x-ray based micro-computed tomography (μCT) measurement technique [15]. The μCT measurement allows for accurate measurement of the cross-sectional geometry of tubular braided structures. Additionally, braided composites are typically exhibit transversely isotropic mechanical properties therefore, mechanics of materials approaches are not valid for examining these structures [16].

Three-dimensional digital image correlation (3D DIC) is another technique relying on the same principles as 2D DIC but uses multiple cameras to obtain more accurate out-of-plane displacement data. Tubular braided composites make a good case for the use of 3D DIC with the undulations of the braid yarns and their curved surface geometry. 3D DIC was used by Wehrkamp-Richter *et al.* to observe deformation of triaxial braids under various types of loading [17]. Leung *et al*. had also used the same technique to observe unit cell behavior of braids during tensile loading [18]. Presently, the 3D DIC method has not been utilized to examine the flexural behavior of braided composite structures.

The objective of this research is to investigate the bending behavior of bio-based biaxial tubular braided composites using 3D DIC. The cross-sectional geometry and void content of the bio-based braids will be assessed using the μCT measurement technique. Braids of varying braid angles manufactured with natural fibers and a bio-based resin will be subjected to 3-point bending loads and design characteristics for ideal bending behavior will be examined.

Experimental Methods

Sample Preparation

Braid Manufacturing

Braid preforms of three nominal braid angles (45, 55, and 65°) were manufactured from regenerated cellulose fibers (BioMid Fiber, 1650 Denier, Burnaby, BC) using a Maypole braiding machine (Steeger USA, K80-72, Steeger USA, Inman, SC). All braid preforms were manufactured using 36 carriers in a Regular (2/2) braid pattern. The mechanical properties of the natural fibers used in this study are summarized in Table 1. Six specimens of each braid angle were prepared for mechanical testing, resulting in a total of eighteen specimens. Aluminum mandrels of 9.525 mm (3/8") diameter were initially covered with 4 layers of wax (Partall Paste #2, Rexco, Conyers, GA) for release of specimens after curing. The preforms were impregnated with a bio-based two-part epoxy resin comprising of an epoxy and a hardener. (SuperSap® ONE/ONF System, Entropy Resins, Inc., Bay City, MI). The epoxy and hardener were mixed in a weight ratio of 100:44. The mechanical properties for the bio-based epoxy are summarized in Table 2. The samples were cured in an oven (Napco 5851-8 Precision Vacuum Oven, Winchester, VA) at 50°C (120°F) for 8 hours with 30-minute-long steps at 32°C and 40°C (90°F and 105°F) before and after the 8-hour long process as per the manufacturer curing cycle. After curing, the samples were cut into a final length of 279.4 mm (10"). Images of the cured braid samples can be seen in Figure 1. This figure shows examples of the three braiding angles (θ) used in this study and the resultant yarn width (W_y) that corresponds to each braid configuration. All braids manufactured in this study were identified using the naming convention of BSSAx/BSSBx/BSSCx. Where A, B, and C represent the braiding angle configuration. Samples were then numbed 1-6 for each braiding configuration resulting in eighteen manufactured samples.

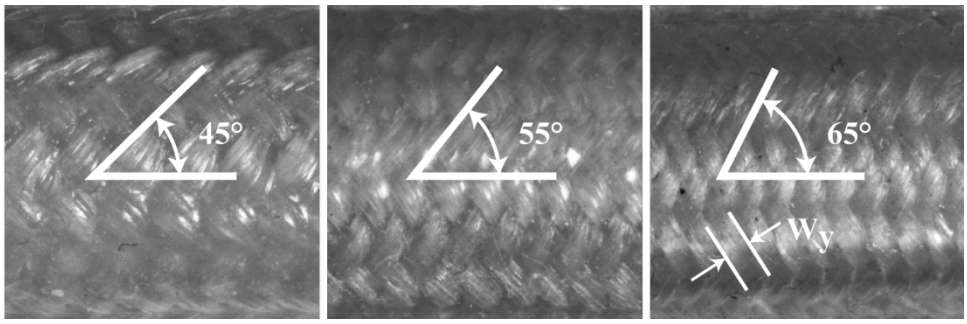

Figure 1: Cured braid sample showing the braid angle (θ) and yarn width (W_y).

Table 1: Mechanical Properties of regenerated cellulose fibers

Mechanical Properties	Reported Data
Elastic Modulus- E_{f1} (GPa)	34.2
Linear Density$\overline{\lambda_m}$ (Denier)	1650
Density ρ (g/cm^3)	1.53

Table 2: Mechanical property data for bio-based epoxy

Mechanical Properties	Reported Data
Tensile Modulus- E_t (GPa)	2.7
Tensile Strength- σ_t (MPa)	53.2
Flexural Modulus- E_f (GPa)	2.5
Flexural Strength- σ_f (MPa)	82.1
Poisson's Ratio- ν	0.3

Braid Geometry Measurement

The external diameters of the cured samples were measured at 10 locations along their length using a micrometer (0-25.4mm Micrometer, Starrett 3732XFL-1, Athol, MA). Additionally, internal diameters were measured at 10 locations throughout the sample, using the same micrometer and a telescoping gauge (8-12mm Telescoping Internal Gauges, KBC Tools, Mississauga, ON).

Each sample was photographed using high resolution cameras (Ace acA2440-35um Monochrome USB 3.0, Basler Inc., Exton, PA) equipped with 50 mm lenses (NMV-50M23, Navitar, Inc., Rochester, NY). Yarn width and braid angle was measured at ten locations for each sample using an image processing software (ImageJ, National Institutes of Health, Bethesda, MD). Example images used for braid angle and yarn width measurements are shown in Figure 1.

Sample Mechanical Testing

The braided samples were evaluated under 3-point bending tests to observe their strain fields under flexure and the fields' variation with different braid angles. A 3-point bending standard does not exist for tubular composite samples but the ASTM D790 Standard Test Methods for Flexural Properties of Unreinforced and Reinforced Plastics and Electrical Insulating Materials was utilized as a guide for determining mechanical testing parameters [19]. Characteristic parameters such as flexural modulus, strength and strain at yield were also calculated using this testing methodology.

Strain throughout the surface of the braided structures vary following the braid pattern. To capture the variation of strain along the surface, a full field strain measurement method, 3D DIC was used during the mechanical tests. For the 3D DIC setup, two high resolution cameras (LaVision Image M-lite 5M, LaVision GmbH, Göttingen, Germany) were used with a resolution of 2464 x 2056 pixels with 10 mm extension tubes (CML10, Thorlabs Inc., Newton, NJ) and 50 mm focal length lenses (NMV-50M23, Navitar, Inc., Rochester, NY), at an f-number of f/16. The cameras were positioned approximately 330 mm away from the specimens. A stereo angle of 20° to maximize

overlap between the two camera images and to maximize the braid sample within the field of view. The imaging setup was designed to obtain a field of view of approximately 46.02 x 38.36mm^2 with an image scale factor of 53.67 pixels/mm, which enabled strain measurement across multiple braid unit cells along the braid length. Both cameras' field of view was centered at the midpoint of the braid specimens, with the braids positioned closer to the top edge of the image to ensure that the specimens remain within the field of view during the entire 3-point test. Images were acquired at a rate of 4 Hz using a commercial software package (DaVis version 10.0.3 StrainMaster, LaVision GmbH, Göttingen, Germany). The test specimen were illuminated using a set of light emitted diode panels (LED Illumination Set, LaVision GmbH, Göttingen, Germany) A schematic of the test setup is shown in Figure 2. In this figure, the stereo camera, test sample, cross-head, and 3-point bending fixture is shown. In addition, the field of view where 3D DIC strain measurement was performed is also shown in this figure.

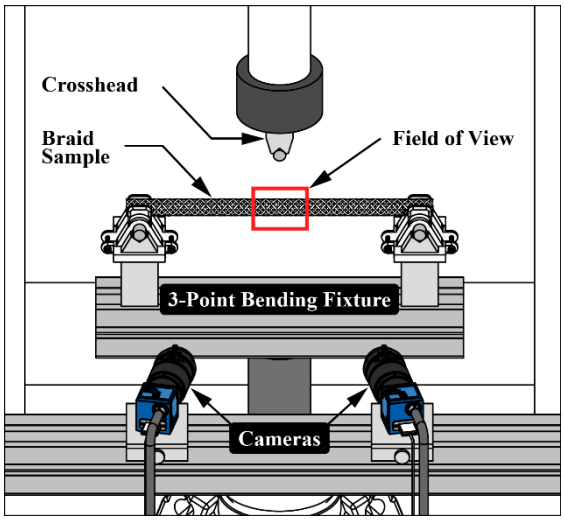

Figure 2: Mechanical testing setup showing the stereo camera system, 3-point bending fixture, tubular braid sample, and field of view of imaging system.

DIC Sample Preparation

A high contrast speckle pattern is necessary for the image correlation process. The speckle contrast pattern and application method for braided composite samples used in this study was adapted from Melenka and Carey [3] [20]. The specimens were initially covered with a gray primer paint (Filler Primer Spray, Rust-Oleum Corp, Concord, ON) to prevent reflections and prepare the specimen surface to ensure uniform surface contrast. A mixture of black paint (5211 Opaque Black, Createx Airbrush Colors, Createx Colors, East Granby, CT) and reducer (4012 High Performance Reducer, Createx) was later applied to the specimens using an airbrush (H-SET, Paasche Airbrush Company, Chicago, IL). The primer paint and speckle colors were chosen to obtain a high contrast, which is required for the DIC algorithm. An example of the speckle pattern applied to the tubular braid samples is shown in Figure 3 (a). A profile of the gray scale variation along the braid length is shown in Figure 3 (b) The speckles applied to the braid sample had an approximate diameter of less than 0.1mm.

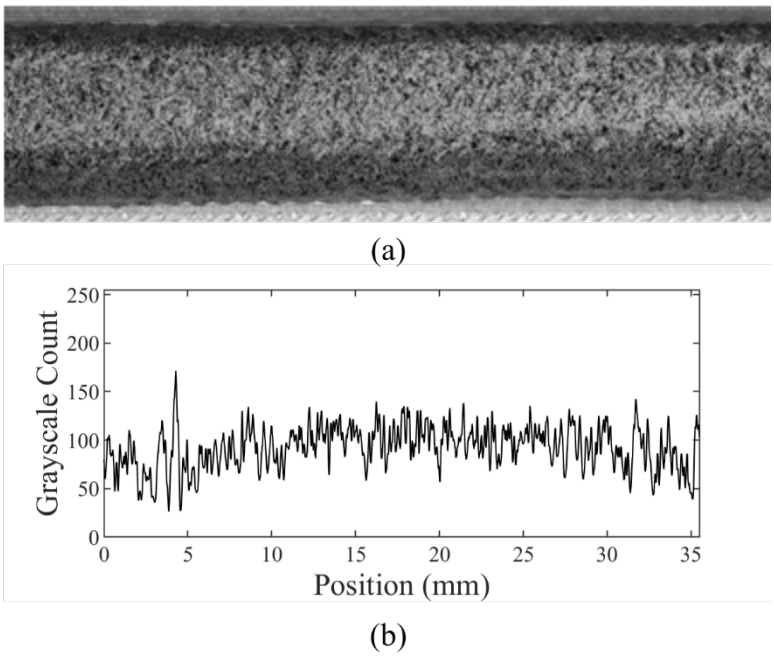

Figure 3: Speckled braid specimen (a) Example braid with applied speckle pattern (b) Profile line demonstrating the grayscale contrast produced by the applied speckle pattern.

Flexural Testing Apparatus

A universal testing machine was used to apply 3-point bending loads to the braid samples (Criterion Model 43, MTS, Eden Prairie, MN, USA). Braid samples were supported with 2 fixed supports with 5 mm radius as per ASTM D790. The flexural testing apparatus and test sample is shown in Figure 4. The supports were positioned to have a 228.6 mm (9”) span. Additional 3D printed supports were added to the sides of the contact surfaces to prevent out-of-plane movement of the specimens. Load data from the test frame were measured using a 250 N capacity load cell (LPB.252 D, MTS, Eden Prairie, MN, USA) and were recorded using a data acquisition system (NI-USB 6211 DAQ, National Instruments, Austin, TX). Braid samples were loaded at a crosshead speed of 1 mm/min.

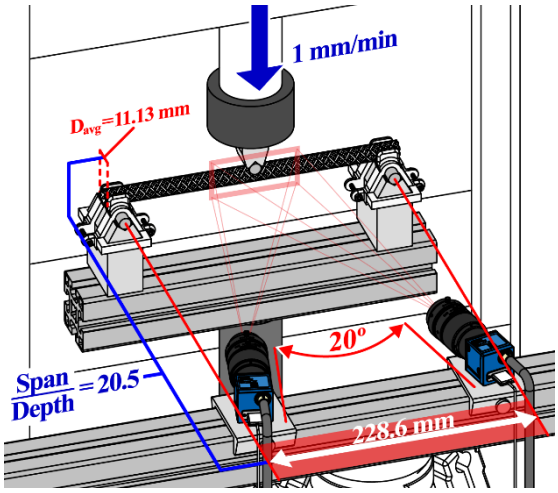

Figure 4: Flexural testing apparatus showing the braid sample, stereo imaging cameras, and position and position of cameras relative to test sample.

3D DIC Processing

A commercial software package was used to process images of the braid samples acquired during bending tests (DaVis version 10.0.3 StrainMaster, LaVision GmbH, Gottingen, Germany). Features in images obtained from the two cameras were linked using a calibration process. A calibration target (Type 058-5-SSDP, LaVision GmbH, Gottingen, Germany) was positioned in the test frame such that its center would coincide with the braid samples' centres. Images of the target are used by the software to determine intrinsic and extrinsic parameters of the cameras [21].

Displacement vector fields were created by using the DIC processing module of the software package, which relies on a Least Squares optical flow displacement measurement algorithm [22]. Subsets of 31x31 pixels were used at a step size of 10 pixels to correlate features between consecutive images. The acquired camera image data and DIC processing parameters are summarized in Table 3.

Table 3: Digital Image Correlation image processing parameters.

Digital Image Correlation Parameters	Settings
Camera Resolution	2464 x 2056 pixels
Camera Pixel Size	3.45 µm
Camera Lenses	2X Navitar 50mm lens with 10mm extension tube
Camera Field of View	46.02 x 38.36mm^2
Image Scale Factor	53.67 pixels/mm
Correlation Subset Size	31 x 31 pixels
Correlation Step Size	10 pixels
Image Acquisition Rate	4 Hz

3D DIC Post-Processing

Displacement vector fields were used to calculate the longitudinal strain (ε_x), transverse (ϵ_y) and shear strain (γ_{xy}) along the tubular braided structures. The longitudinal and transverse directions are defined in Figure 5 with respect to the longitudinal axis of the tubular braid sample.

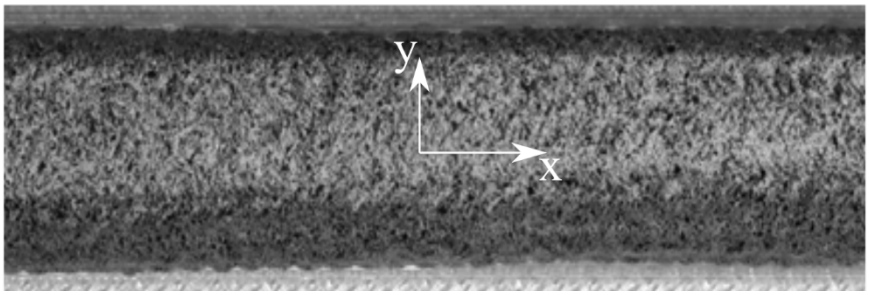

Figure 5: Tubular braid coordinate system. Longitudinal (x) and transverse strain (y) axes

Void and Cross-Section Measurement

A high resolution micro-computed tomography technique was used to evaluate void content and cross-sectional geometry of the natural fiber/ bio-based resin braided composite structures. One sample of each braid configuration (BSSA, BSSB, BSSC) was examined using the µCT analysis technique. The braid samples were evaluated using a SkyScan 1272 microtomograph (Bruker-MicroCT, Kontich, Belgium). The settings for the µCT scan of each braid sample are detailed in Table 4. The settings shown in Table 4 were selected to optimize contrast between the matrix and fiber materials. A voxel size of 3.0 µm was selected to maximize the braid sample diameter within the field of view. The complete details of the void analysis procedure is described by Melenka *et al.* [7]. The radiograph images collected from the µCT scanner were reconstructed to create cross-sectional images of the braid samples (NRECON 1.7.1.0, Bruker, Belgium). The resultant cross-sectional images were used for analysis of the braided geometry and void content. An example reconstructed braid cross-section is shown Figure 6. In this image the resin and fibers can be identified through variations in grayscale contrast. Voids within the braid cross-section can also be seen. Additionally, the primer paint used to prepare the surface of the braids for DIC analysis can also be seen around the outside perimeter of the sample.

Table 4: Micro-computed tomography (µCT) scan parameters

µCT Parameter	Value
X-Ray Voltage	40 kV
Current	200 µA
Frame Averaging	4
Rotation Step	0.1°
Number of Projections	1920
Projection Exposure Time	529 ms
Detector Pixel Size	7.4 µm
Reconstructed Image Pixel Size	3.0 µm
Image Resolution	4904x3280 pixels
Scan Time	155 minutes

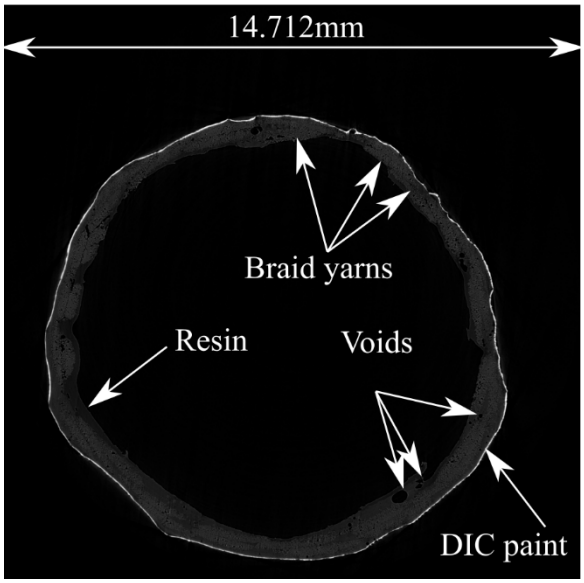

Figure 6: Reconstructed braid cross-section showing resin, fibers, voids, and external surface paint for DIC analysis

The identification process for voids within the braid samples is shown in Figure 7. An example braid cross-section is shown in Figure 7 (a). Voids were identified using a custom image analysis script (MATLAB 2018a, The MathWorks, Natick, Mass). Voids in the braid samples were identified by using the "im2bw" thresholding command in MATLAB (Figure 7 (b)) using a grayscale threshold of 12-255. All voids were removed from the segmented image to allow for individual void identification using the "imfill" MATLAB function. The thresholded braid cross-section was subtracted from the filled cross-section to obtain the final void distribution (Figure 7 (c)). The generated binary images shown in Figure 7 allow for the size and distribution of voids and pores to be analyzed throughout the 3D braid geometry.

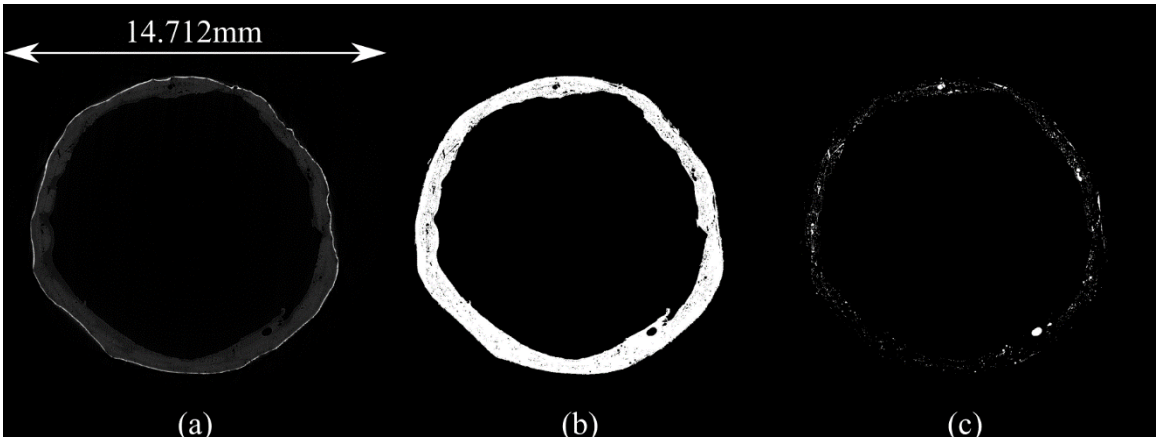

Figure 7: Braid void segmentation procedure (a) original braid cross-section, (b) thresholded cross-section showing voids, (c) identified voids within braid cross-section

The braid cross-sections shown in Figure 7 were also analyzed to calculate the area moment of inertia of the braid sample. Image processing software (ImageJ, National Institutes of Health, Bethesda, MD) and corresponding plugin "BoneJ2" was utilized to calculate the area moment of inertia of the braid cross-sections.

Results and Discussion

Braid Geometry Analysis

External (D_o) and internal (D_i) diameter as well as braiding angle measurements were collected for all samples investigated in this study. Internal and external diameter measurements are required to compute the second moment of area, I, of the braid samples. The inner and outer diameters of the braid samples were measured using a high-resolution micrometer. The equation for the second moment of area for the braided samples is shown in equation (1). The area moment of area shown in equation (1) will be used to compute bending stress applied to the tubular braid samples.

$$I = \frac{\pi}{64}(D_0^4 - D_i^4) \quad (1)$$

Braiding angle was also measured as the mechanical properties of braided composites are highly sensitive variations in braid angle [23]. The average braiding angle of the 3 groups of manufactured samples were found to be 46.2, 55.6 and 63.5° respectively. Measurement of the braid samples are summarized in Table 5. Average and standard deviations for braiding angle, yarn width, internal, and external diameters are reported for all manufactured samples.

Table 5: Average braid angles of specimens and standard deviations

Specimen	Braid Angle θ (°)		Yarn Width- W_y (mm)		Measured Internal Diameter D_i (mm)		Measured Outer Diameter D_o (mm)	
	Avg	StDev	Avg	StDev	Avg	StDev	Avg	StDev
BSSA1	46.16	1.78	1.280	0.141	10.44	0.35	11.69	0.27
BSSA2	44.22	2.74	1.341	0.097	10.10	0.18	11.32	0.18
BSSA3	48.41	2.90	1.429	0.143	10.29	0.32	11.33	0.47
BSSA4	47.27	3.53	1.557	0.097	10.35	0.33	11.14	0.24
BSSA5	44.63	3.08	1.482	0.135	10.28	0.14	11.70	0.33
BSSA6	46.63	2.67	1.636	0.115	10.49	0.16	11.59	0.36
BSSB1	56.61	2.14	1.085	0.061	9.64	0.06	10.97	0.32
BSSB2	56.72	2.72	1.075	0.036	9.73	0.04	10.94	0.18
BSSB3	54.66	4.19	1.152	0.082	9.97	0.15	11.14	0.17
BSSB4	55.49	2.43	1.196	0.085	9.80	0.16	10.88	0.17
BSSB5	55.82	2.69	1.185	0.077	9.76	0.12	11.08	0.21
BSSB6	54.42	3.12	1.149	0.076	9.78	0.09	10.88	0.17
BSSC1	63.23	2.37	0.757	0.049	9.61	0.09	11.03	0.16
BSSC2	64.58	3.39	0.846	0.045	9.56	0.05	11.11	0.23
BSSC3	60.91	3.57	0.898	0.063	9.60	0.03	10.85	0.19
BSSC4	63.68	2.14	0.902	0.051	9.57	0.04	10.85	0.08
BSSC5	63.69	3.06	0.875	0.052	9.60	0.06	10.70	0.15
BSSC6	65.05	2.92	0.878	0.044	9.62	0.14	11.10	0.18

The inner and outer braid diameters reported in Figure 5 were used to calculate the area moment of inertia of the braid samples. The area moment of inertia was calculated using equation (1). The area moment of inertia is required to calculate the bending stress for the tubular braid samples. For comparison the area moment of inertia of the braid samples was also determined using the µCT analysis technique from the 2D cross-sections of the braid sample. Comparison of the physically measured area moment of inertia and using the non-contact µCT analysis technique are compared in Table 6. This table shows that there is a significant difference in the area moment of inertia of the tubular braid samples between the two measurement methods. As a result, the physical measurements of the braid samples may underestimate the actual area moment of inertia of the braid samples. This will have an effect on the calculation of the bending stress within the braid sample and consequently calculation of the flexural modulus. Although the µCT approach may allow for better evaluation of the cross-sectional geometry of the tubular braid samples, this process may not be practical for large scale measurement of braid samples due to cost constraints associated with the µCT measurement approach.

Table 6: Comparison of Area Moments of Inertia measured using a standard physical measurements and using the μCT measurement method

Braid Sample	Nominal Braid Angle	Area Moment of Inertia (mm^4)			
		Micrometer		µCT	
		Avg	StDev	Avg	StDev
BSSA6	45°	290.40	61.43	414.47	12.68
BSSB6	55°	265.40	23.74	332.01	5.57
BSSC6	65°	287.92	42.21	530.09	9.65

Bending Test Results

Representative Strain Images

The 3D DIC measurement method allow for full field displacement and strain measurement of the tubular braid samples. Figure 7 and Figure 8 shows representative longitudinal and transverse strain fields for braids of varying braid angle for loads of 5, 7 and 10N. Variations in strain throughout the surfaces of tubular braids of different braid angles. Additionally, Figure 9 shows representative shear strain for the tubular braids at varying braid angles and applied loads.

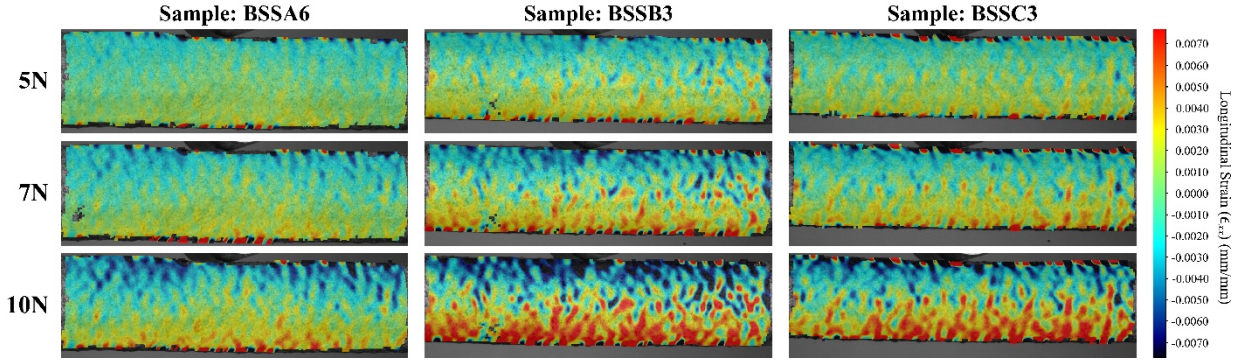

Figure 8: Representative longitudinal strain fields (ϵ_{xx}) for braided composite samples under bending.

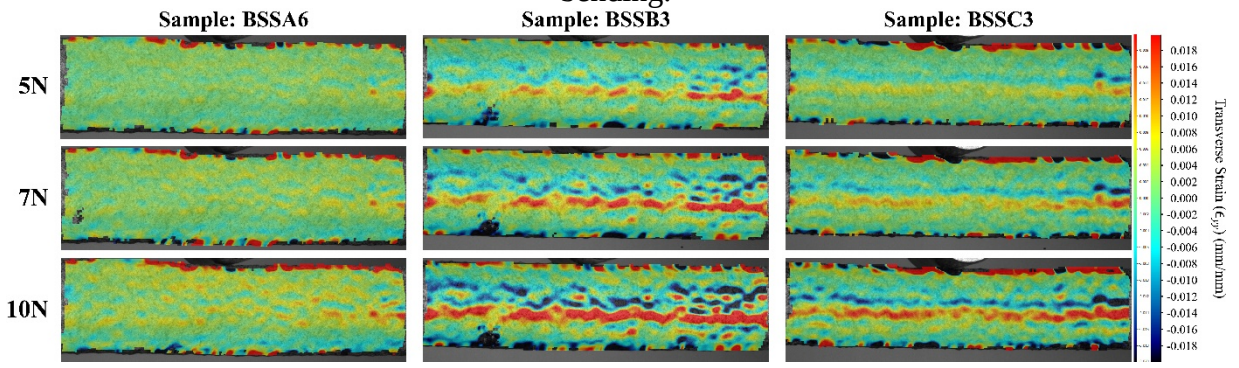

Figure 9: Representative transverse strain fields (ϵ_{yy}) for braided composite samples under bending.

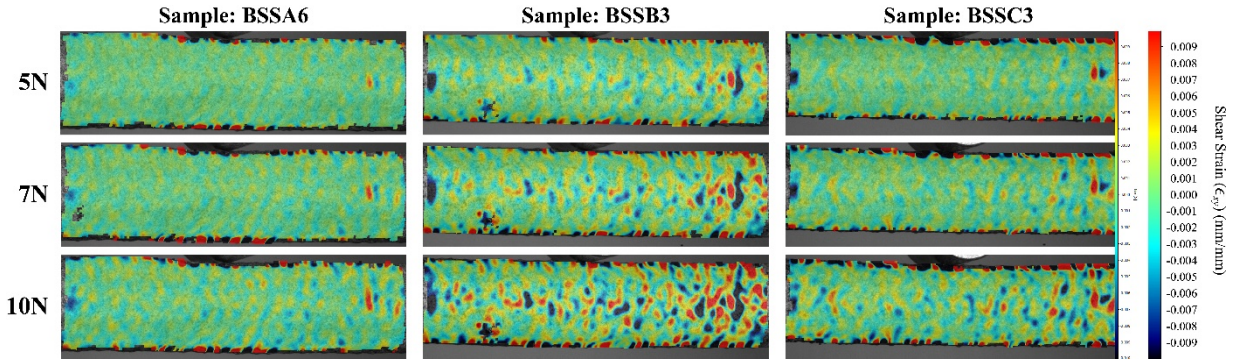

Figure 10: Representative shear strain fields (ϵ_{xy}) for braided composite samples under bending

The magnitude of strain changes periodically along the braid surfaces with respect to the braiding pattern, with regions of tensile strains followed by regions of compressive strains on the neighboring yarn and vice versa. This pattern is clearly visible in Figure 10, which displays the variation of strain with respect to longitudinal position along 3 lines placed near the top surface, neutral axis and the bottom surface. As bottom surface experiences tension during bending, strains fluctuate around a positive mean value. The mean strain is negative for the line drawn near the top surface, since compressive strain is experienced. The line along the neutral axis has a near-zero mean with fluctuations of higher magnitude. As load on the structure increases, magnitude of strains intensifies, indicated by richer shades of red and blue on the strain fields corresponding to higher loads. Previous studies have examined braided composite structures under flexural loading, however the effect of the non-uniform geometry and strain fields like the ones shown in Figure 10 were not taken into account [4]. Similar strain field variations have been observed by Melenka and Carey for tubular braid samples under tensile and torsional loading [20].

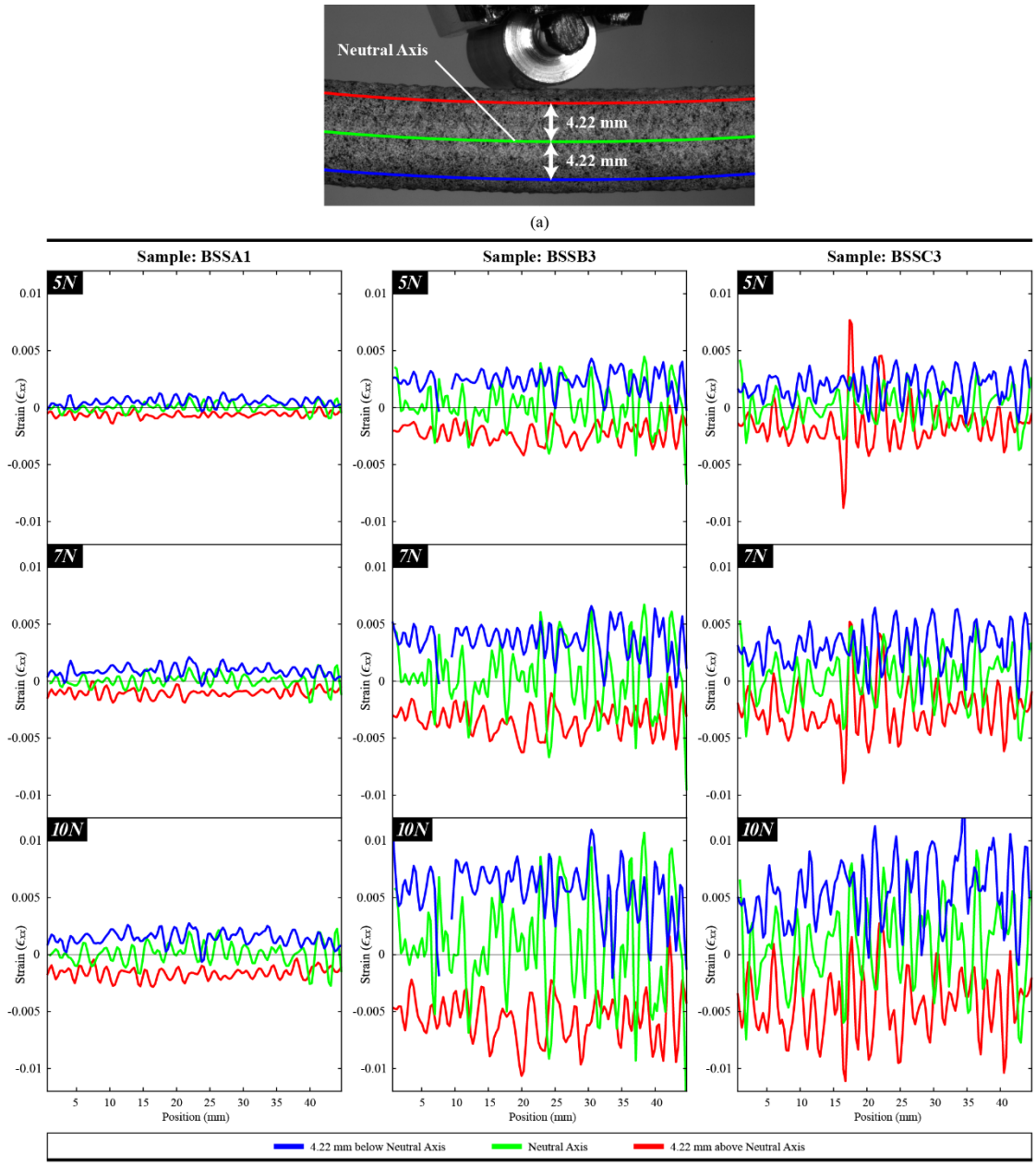

Figure 11: Strain variation along longitudinal axis of tubular braided composite sample. (a) Example braid sample with Three locations selected to visualize braid strain 4.2mm above the neutral axis (blue), along the sample neutral axis (red) and 4.22mm below the neutral axis (green) (b) Resultant longitudinal strain ϵ_{xx} along the braid longitudinal axis.

The effect of braiding angle on resultant stain versus load can be seen in Figure 11. Representative strain regions with size 6.41 x 2.75 mm^2 were selected at three locations along the mid-span of braid specimens of different braid angles. Strain regions were positioned to have their center at the neutral axis (green), 3.45 mm above the neutral axis (red) and 3.45 mm below the neutral axis (blue) as shown in Figure 11 (a). These regions were selected to calculate the average tensile and compressive strain for the tubular braid sample as well as to examine the strain at the neutral axis.

Representative average strain verses applied load (P) plots are shown in Figure 11 (b). Maximum bending stresses below the neutral axis of the test specimens were calculated using load data and specimen specific geometry data.

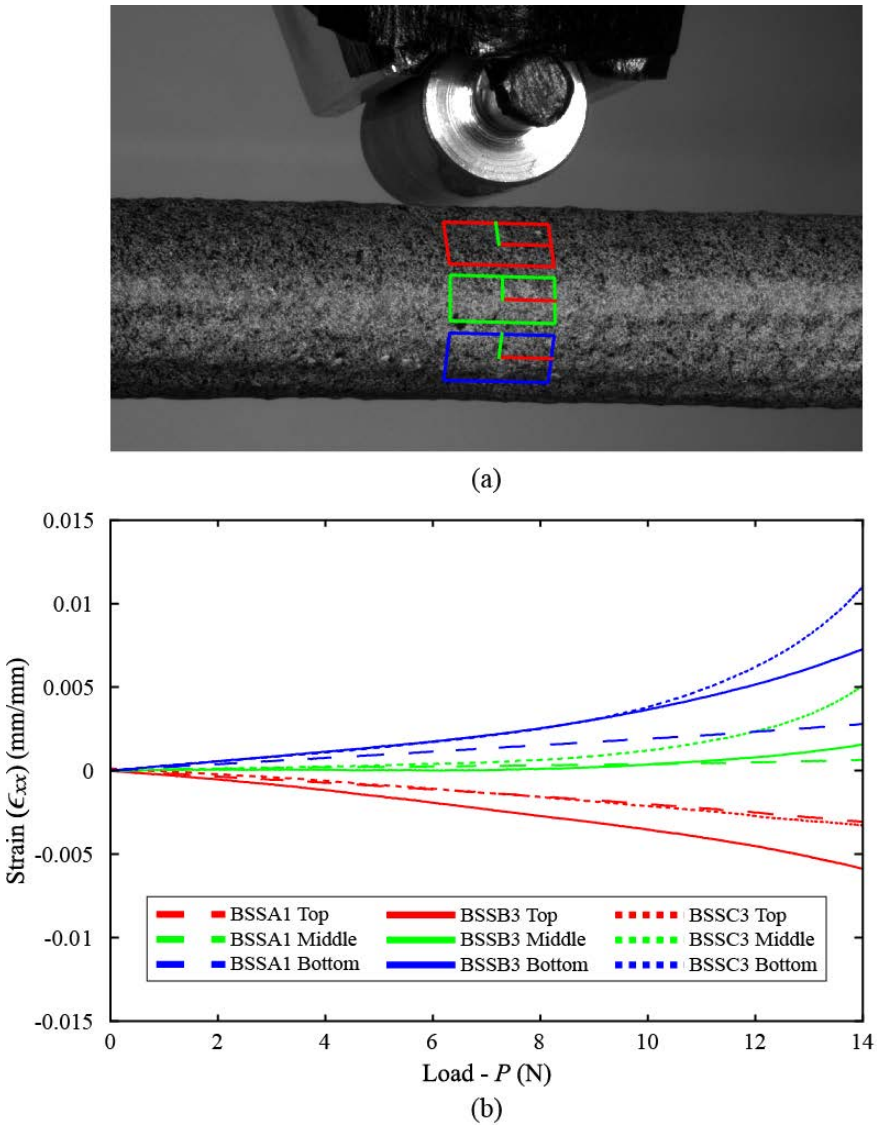

Figure 12: Average bending strain of tubular braid samples (a) Strain calculation regions Above neutral axis-red, Neutral axis-green, Below neutral axis-blue (b) Plot of sample strain versus applied load

Stress-Strain Plots

Plots of load verses cross-head displacement for the three braid sample configurations is shown in Figure 12. The effect of braiding angle on braid deflection can be seen in this figure. These plots show the resultant bending load, P, verses cross-head displacement, δ for the 45, 55 and 65° braid samples. The collected load and displacement data was then used to calculate the bending stress σ_b for the tubular braids. Average tensile strain was computed using a rectangular region below the neutral as shown in Figure 11.

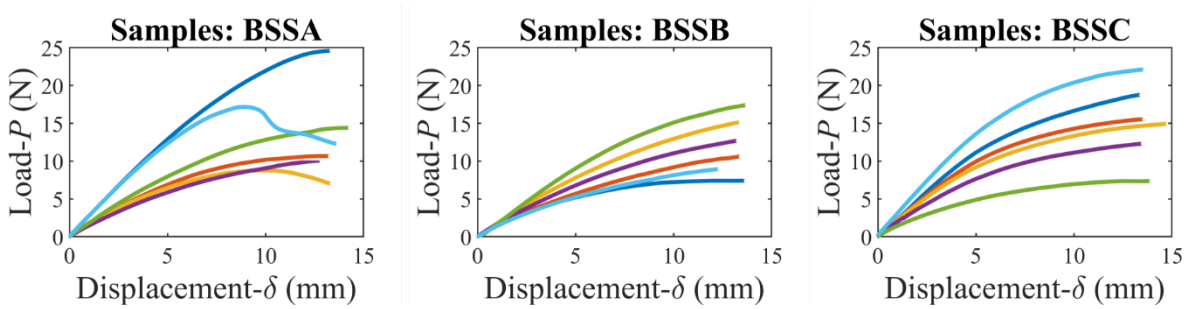

Figure 13: Load vs cross-head displacement of tubular braid samples (a) 45° (b) 55° (c) 65°

Bending stress, σ_b, for each sample was calculated using equation (2) where P is the measured applied force, L is the span of the 3-point bend fixture and D_o is the sample outer diameter and D_i is the inner diameter.

$$\sigma_b = \frac{8\,P\,L\,D_o}{\pi(D_o^4 - D_i^4)} \tag{2}$$

Resultant plots of bending stress, σ_b, versus tensile strain ϵ are shown in Figure 13. The average tensile strain was determined using the representative region shown in Figure 11. This figure shows the effect of braiding angle on bending behavior of 45, 55 and 65° tubular braid samples.

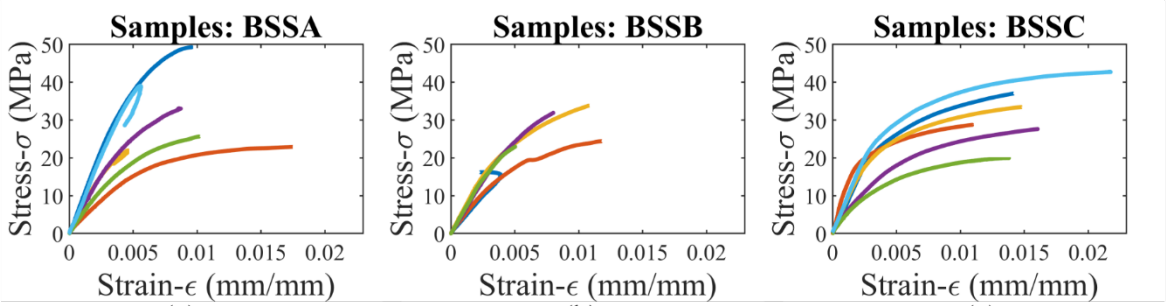

Figure 14: Stress versus strain of tubular braid samples (a) 45° (b) 55°(c) 65°

Flexural Moduli

The bending stress-strain curves shown in Figure 13 were used to compute the flexural moduli for the 45, 55 and 65° tubular braid samples. The flexural modulus was calculated using the Tangent Modulus of Elasticity using the method described in ASTM D790 [19]. The resultant flexural moduli for the three sample configurations investigated in this study are shown in Figure 14. In this figure, the average flexural modulus for each of the braiding angle is shown as well as the standard deviation. The flexural moduli for the three braid sample configurations were found to be 6.10±2.14, 5.07±1.07, and 6.66±2.63 GPa for the 45, 55 and 65° nominal braid angle configurations respectively.

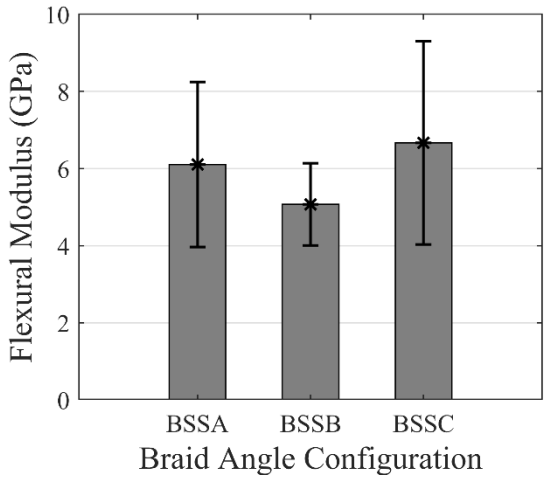

Figure 15: Comparison of flexural moduli for tubular braided composite samples

The resultant flexural moduli reported in Figure 15 demonstrate that significant variations within the tubular braid samples exist. Similar variations were also observed by Potluri *et al.* [4]. Variations in the expected flexural moduli from conventional results from mechanics of materials may be attributed to the influence of the fiber volume fractions that exist within the tubular braid samples. As braiding angle increases, the fiber volume fraction increases as well. As a result, fiber volume fractions may have an additional influence on the flexural modulus of the tubular braid samples.

The study by Potluri *et al.* utilized 274 tex E-glass yarns manufactured using a 24-carrier braiding machine [4]. Braids were manufactured using a mandrel diameter of 6mm with braiding angles of 31, 45 and 65° braid angles. Results for the flexural modulus obtain by Potluri *et al.* are compared with the flexural moduli obtained in this study. This comparison is shown in Figure 16. Braids used in this study were produced using 1650 denier regenerated cellulose fibers using a 36 carrier braiding machine and braided using a . This figure demonstrates that comparable flexural modulus results can be obtain for E-glass and regenerated cellulose fibers for braided composite structures.

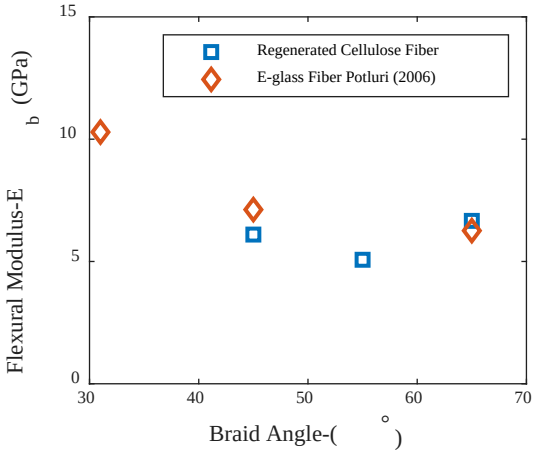

Figure 16: Comparison of flexural moduli of braided composite structures. Braid samples were produced using E-glass fibers *[4]* and regenerated cellulose fibers.

Additionally, an idealized cross-sectional geometry was utilized to calculate the area moments of inertia for each of the tubular braid samples. Comparison of the area moments of inertia calculated using conventional measurement methods and using the contact free µCT approach shown in Table 6 show that significant differences for the sample braid sample exist between the two measurement approaches. Calculation of the area moment of inertia for the braid samples will have a significant effect on the calculated bending stress and resultant flexural moduli. A comparison of the influence on the measured area moment of inertia on flexural modulus for three of the tubular braid samples is shown in Table 7. This table demonstrates that measurement of the braid geometry will have an effect on the calculated flexural modulus for the tubular braid samples.

Table 7: Comparison of flexural moduli using micrometer and uCT measurement approaches to calculate the area moment of inertia of the tubular braid samples

Sample	Flexural Modulus (GPa) Micrometer Area Moment of Inertia	Flexural Modulus (GPa) µCT Area Moment of Inertia	Percent Difference (%)
BSSA6	8.010	8.348	4.05
BSSB6	5.904	5.953	0.82
BSSC6	7.670	8.116	5.50

Braid Void Content

Example void distributions for three braid samples (45°, 55°, and 65° nominal braid angles) are shown in Figure 17. The effect of braiding angle on the distribution throughout each braid sample can be seen in each of the three dimensional images.

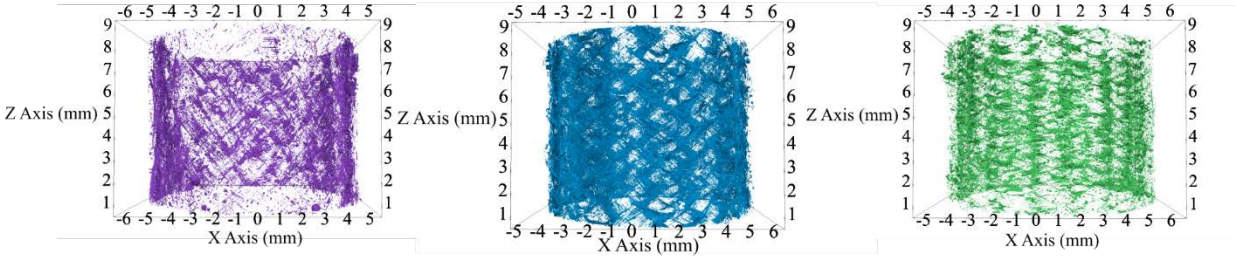

(a) (b) (c)

Figure 17: Void content of natural fiber braided composites (a) BSSA6 Sample (b) BSSB6 Sample (c) BSSB6 Sample

Using an image segmentation procedure, the resin, fibers and voids within the three braid samples was identified. Resin and fibers were identified base on their differences in density. This approach allows for the total volume of each constituent within the braid sample to be calculated. The resultant fiber, matrix and void volumes for the three samples are summarized in Table 8. Table 8 shows that there is an increase in fiber volume and fiber volume fraction as braiding angle increases. Additionally, variations in the matrix volume fraction for the three braid samples can be observed in Table 8. Variations in matrix volume fractions can be attributed to the higher fiber volume fractions of the braid samples. As braiding angle increases, the braid fiber yarns reach a jammed state where braiding angle can no long increase. At the jam angle, the braid yarns become compacted which will affect the permeation of resin within the braid yarns. As a result, braiding angle has an influence on both the resin and fiber volume fractions exhibited by the braid samples summarized in Table 8. The void distribution examined for the manufactured braid samples will also influence the mechanical properties of the braid samples examined in this study.

Table 8: Braid calculated fiber, matrix and void volumes

Sample	BSSA6	BSSB6	BSSC6
Measured Braid Angle (°)	46.63	54.42	65.05
Fiber Volume V_f (mm^3)	87.11	95.17	157.25
Matrix Volume V_m (mm^3)	105.36	71.84	109.53
Total Void Volume (mm^3)	8.88	15.7	12.36
Total Volume (mm^3)	201.36	182.74	279.14
Fiber Volume Fraction v_f	43.26%	52.08%	56.33%
Matrix Volume Fraction v_m	52.33%	39.31%	39.24%
Total Void Volume Fraction v_T	4.41%	8.61%	4.43%

Conclusions

This study has assessed the flexural properties of bio-based braided composite structures using the 3D DIC strain measurement technique. Braid samples were manufactured using regenerated

cellulose fibers and embedded within a bio-based resin. The effect of three-point bending on the resultant strain field for the bio-based braid samples was assessed. The flexural modulus was determined for three braid angle configurations. The determined flexural moduli were 6.10±2.14, 5.07±1.07, and 6.66±2.63 GPa for the BSSA (45°), BSSB (55°) and BSSC (65°)configurations examined in this work. Non-uniform strain field were observed for the tubular braid samples. Strain for the tubular braid samples was shown to be effected by both braiding angle and the position relative to the neutral axis of the braid sample. The non-uniform strain fields observed using the 3D DIC measurement technique demonstrates that full field strain measurement methods are necessary to examine the strain fields for tubular braided composite structures.

The cross-sectional geometry of the three braided configurations was also examined using a µCT measurement method. The fiber volume fractions for the three braid configurations was determined to be 43.26%, 52.08%, and 56.33% for the BSSA (45°), BSSB (55°) and BSSC (65°) braid configurations. Additionally, void volume fractions were determined to be 4.41%, 8.61% and 4.43% for the three examined braids. Cross-sectional geometry of the braided samples was assessed using both physical measurements and the µCT measurement method. Significant differences in the braid area moment of inertia were found between physical measurements and the µCT. The µCT measurement method will provide a more accurate representation of the cross-sectional geometry of tubular braided structures however this technique is costly and time intensive compared to conventional physical measurement methods.

This work demonstrates that the flexural properties of braided composite structures can be influenced by a number of manufacturing parameters. The flexural properties of braided structures will be influence by the braiding angle, area moment of inertia, and void content within the braid structure. The influence of these parameters on braid mechanical properties must be considered for the design of braided structures under flexural loads. Utilization of consolidation methods such as vacuum bagging or shrink wrap tape will help reduce the void content of braided structures and produce more consistent braid geometries. By reducing void content and improving braid cross-sectional geometry more consistent performance of braided composite structures can be achieved.

Acknowledgments

The authors would like to express their gratitude to Ms. Bruni-Bossio for producing the braid preforms and Dr. Ayranci and Dr. Carey for providing the sample materials used in this study. The authors would also like to thank Dr. Czekanski for the use of the MTS test frame in this work. The authors would like to acknowledge the funding support of the Natural Science and Research Council (NSERC) Canada RGPIN-2018-05899.

Bibliography

[1] G. W. Melenka *et al.*, “Manufacturing processes for braided composite materials,” in *Handbook of Advances in Braided Composite Materials: Theory, Production, Testing and Applications*, 2016, pp. 47–153.

[2] C. Ayranci and J. Carey, “2D braided composites: A review for stiffness critical

applications," *Compos. Struct.*, vol. 85, no. 1, pp. 43–58, Sep. 2008.

[3] G. W. Melenka and J. P. Carey, "Experimental analysis of diamond and regular tubular braided composites using three-dimensional digital image correlation," *J. Compos. Mater.*, vol. 51, no. 28, pp. 3887–3907, 2017.

[4] P. Potluri, A. Manan, M. Francke, and R. J. Day, "Flexural and torsional behaviour of biaxial and triaxial braided composite structures," *Compos. Struct.*, vol. 75, no. 1–4, pp. 377–386, Sep. 2006.

[5] C. Ayranci and J. P. Carey, "Effect of diameter in predicting the elastic properties of 2D braided tubular composites," *J. Compos. Mater.*, vol. 44, no. 16, pp. 2031–2044, 2010.

[6] I. I. Qamhia, S. S. Shams, and R. F. El-Hajjar, "Quasi-Isotropic Triaxially Braided Cellulose-Reinforced Composites," *Mech. Adv. Mater. Struct.*, vol. 22, no. 12, pp. 988–995, 2015.

[7] G. W. Melenka, B. M. Bruni-Bossio, C. Ayranci, and J. P. Carey, "Examination of voids and geometry of bio-based braided composite structures," *IOP Conf. Ser. Mater. Sci. Eng.*, vol. 406, p. 012012, 2018.

[8] B. Bruni-bossio, C. Ayranci, J. Carey, T. Omonov, and J. Curtis, "Experimental testing of the tensile elastic properties of cellulose braided composites," *Compos. Part B Eng.*, vol. 166, no. February, pp. 542–548, 2019.

[9] N. Saheb and J. Jog, "Natural Fiber Polymer Composites : A Review," *Adv. Polym. Technol.*, vol. 2329, no. July, pp. 351–363, 2015.

[10] R. Sturm and F. Heieck, "Energy absorption capacity of braided frames under bending loads," *Compos. Struct.*, vol. 134, pp. 957–965, 2015.

[11] Y. Zhong, R. Suraj, C. Wang, E. S. M. Chia, S. C. Joshi, and Z. Chen, "Damage advancement behavior in braided composite structures for mini aerial vehicles," *Mech. Adv. Mater. Struct.*, vol. 25, no. 11, pp. 889–900, 2018.

[12] G. Liu *et al.*, "Inverse identification of tensile and compressive damage properties of graphite material based on a single four-point bending test," *J. Nucl. Mater.*, vol. 509, pp. 445–453, 2018.

[13] P. Planques *et al.*, "Characterization of the mechanical properties of thermal barrier coatings by 3 points bending tests and modified small punch tests," *Surf. Coatings Technol.*, vol. 332, no. September, pp. 40–46, 2017.

[14] T. Voiconi, E. Linul, L. Marşavina, T. Sadowski, and M. Kneć, "Determination of Flexural Properties of Rigid PUR Foams Using Digital Image Correlation," *Solid State Phenom.*, vol. 216, no. October 2013, pp. 116–121, 2014.

[15] G. W. Melenka, E. Lepp, B. K. O. Cheung, and J. P. Carey, "Micro-computed tomography analysis of tubular braided composites," *Compos. Struct.*, vol. 131, pp. 384–396, 2015.

[16] G. W. Melenka and J. P. Carey, "Development of a generalized analytical model for tubular braided-architecture composites," *J. Compos. Mater.*, 2017.

[17] T. Wehrkamp-Richter, R. Hinterhölzl, and S. T. Pinho, “Damage and failure of triaxial braided composites under multi-axial stress states,” *Compos. Sci. Technol.*, vol. 150, pp. 32–44, 2017.

[18] C. K. Leung, G. W. Melenka, D. S. Nobes, and J. P. Carey, “The effect on elastic modulus of rigid-matrix tubular composite braid radius and braid angle change under tensile loading,” *Compos. Struct.*, vol. 100, pp. 135–143, 2013.

[19] ASTM Standards, “D790−15 Standard Test Methods for Flexural Properties of Unreinforced and Reinforced Plastics and Electrical Insulating Materials,” *Annu. B. ASTM Stand.*, pp. 1–12, 2015.

[20] G. W. Melenka and J. P. Carey, “Experimental analysis of diamond and regular tubular braided composites using three-dimensional digital image correlation,” *J. Compos. Mater.*, pp. 1–21, 2017.

[21] “A Good Practices Guide for Digital Image Correlation,” no. January. International Digital Image Correlation Society, 2018.

[22] LaVision GmbH, “Product-Manual DaVis StrainMaster 10.0 Item-Number(s): 1003017.” LaVision GmbH, Göttingen, 2018.

[23] J. Chen, T. McBride, and S. Sanchez, “Sensitivity of Mechanical Properties to Braid Misalignment in Triaxial Braid Composite Panels,” *J. Compos. Technol. Res.*, vol. 20, no. 1, pp. 13–17, 1998.